

Spectrotemporal shaping of attosecond x-ray pulses with a fresh-slice free-electron laser

River R. Robles,^{1,2,3,*} Kirk A. Larsen,^{1,3,†} David Cesar,¹ Taran Driver,^{1,3} Joseph Duris,¹ Paris Franz,^{1,2,3} Douglas Garratt,^{1,3} Nicholas Sudar,¹ Jun Wang,^{1,2,3} Zhen Zhang,¹ James Cryan,^{1,3,‡} and Agostino Marinelli^{1,3,§}

¹*SLAC National Accelerator Laboratory, Menlo Park, CA 94025*

²*Stanford University, Department of Applied Physics, Stanford, CA 94305*

³*Stanford PULSE Institute, SLAC National Accelerator Laboratory, Menlo Park, CA 94025, USA*

(Dated: March 5, 2024)

We propose a scheme for coherently shaping attosecond x-ray pulses at free-electron lasers. We show that by seeding an FEL with a short coherent seed that overfills the amplification bandwidth, one can shape the wigner function of the pulse by controlling the undulator taper profile. The examples of controllable coherent pulse pairs and trains, as well as isolated spectrotemporally shaped pulses with very broad coherent bandwidths are examined in detail. Existing attosecond XFELs can achieve these experimental conditions in a two-stage cascade, in which the coherent seed is generated by a short current spike in an electron bunch and shaped in an unspoiled region within the same bunch. We experimentally demonstrate the production of pulse pairs using this method at the Linac Coherent Light Source.

Optical lasers have had a far reaching impact on modern science and society. Key to their broad success has been the development of coherent shaping methods that allow the production of waveforms with programmable amplitude, phase, frequency, and pulse format [1–5]. Such control has many different forms and applications. Control over the time-dependent phase of an optical pulse enables, for example, chirped pulse amplification, whose broad scientific impact is so significant that it was recently recognized with a Nobel prize [6]. Coherent shaping of laser pulses has more fundamental scientific applications in coherent control, in which engineering the precise amplitude and phase of an optical pulse is used to exert control over the dynamics of a quantum system [7–11].

Free-electron lasers (FELs) have extended our access to high intensity coherent radiation sources into the extreme ultraviolet (EUV) and x-ray regions [12–14]. EUV FELs, in particular, benefit from conventional laser technology since they can be seeded by external lasers in harmonic generating schemes [15–19]. Externally seeded FELs transfer the coherence in the seed laser to the EUV pulse. Combined with the inherent flexibility of FEL systems, seeding enables a variety of coherent shaping methods [20, 21]. To date, several coherent shaping possibilities have been demonstrated at EUV FELs: the production of phase correlated two-color pulses [22], stable attosecond pulse trains [23], and chirped pulse amplification [24].

X-ray FELs typically operate in the self amplified spontaneous emission (SASE) mode, in which the FEL interaction is seeded by shot noise in the electron beam.

As such, SASE light is typically temporally incoherent, composed of a number of uncorrelated temporal and spectral spikes. Shaping of SASE x-ray pulses has been achieved by shaping the phase-space of the electron bunch, resulting in multicolor FELs [25, 26], and pulses of variable duration and structure [27–29], down to the attosecond regime [30–32].

In this letter, we propose a coherent spectrotemporal shaping method for attosecond XFEL pulses. Leveraging the interplay between slippage and the finite FEL gain bandwidth, we show that the coherent bandwidth of an isolated attosecond pulse can be manipulated to produce a wide variety of output pulses with different spectrotemporal characteristics. Unlike other proposed methods at x-ray energies, our approach enables both amplitude and phase shaping. Since our method utilizes a spectrally coherent seed – an initial isolated attosecond pulse – the resulting shaped pulses intrinsically inherit that coherence. This method enables a variety of new experimental techniques, ranging from bandwidth broadening for impulsive stimulated X-ray Raman scattering [33], to the realization of advanced beam microbunching schemes for the production of shorter attosecond pulses [34]. Additionally, the proposed method enables the generation and shaping of electronic wavepackets beyond the impulsive limit [35], providing a path to understanding the coupling and interplay between electronic and nuclear dynamics in complex molecules.

Our proposed shaping method is illustrated in Figure 1. First, a current spike in the driving electron beam produces an isolated attosecond pulse in an initial undulator stage (a). We will refer to this first attosecond pulse as the “seed pulse” throughout the paper. This is the standard method for producing isolated attosecond pulses at XFELs and can be achieved with a variety of beam manipulation techniques [30, 36–38]. The beam is then delayed with respect to the seed in a magnetic chicane (b). The seed pulse is now overlapped with a

* riverr@stanford.edu

† larsenk@stanford.edu

‡ jcryan@slac.stanford.edu

§ marinelli@slac.stanford.edu

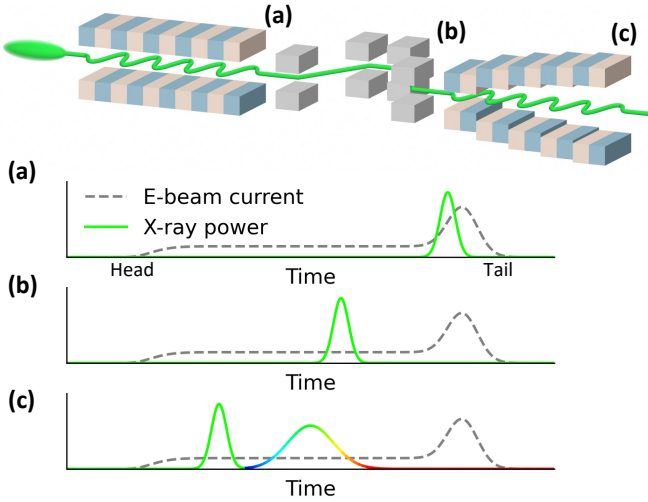


FIG. 1. A basic illustration of the scheme to shape the spectrotemporal profile of attosecond pulses. An isolated attosecond pulse produced in one undulator stage (a) is slipped onto a fresh part of the electron beam in a magnetic chicane (b). Varying the taper of the undulator in this second stage enables time-dependent control of the e-beam microbunching frequency and subsequent x-ray emission (c). In (a)-(c), the head of the beam is at the left.

“fresh” slice in a lower current portion of the bunch, i.e. a slice that was not spoiled by the FEL process in the first stage. The attosecond pulse then acts as a coherent seed for lasing in a second stage, in which by varying the taper of the undulator we can produce a second pulse with a flexible spectrotemporal structure (c). The physical mechanism behind this spectrotemporal shaping is an interplay between slippage and the finite bandwidth of the seed’s modulation of the e-beam energy. As the seed pulse slips over the e-beam it modulates the energy of the slices it passes over. The resulting energy modulation occurs at a frequency that corresponds to the local undulator resonance condition. This time-dependent energy modulation is then converted into a time-dependent density modulation by the undulator dispersion, and is used to produce an x-ray pulse with the same spectrotemporal shape.

We can understand the basic relationship between the induced microbunching and the undulator taper using the one-dimensional collective variables model of the FEL interaction. The collective variable equations can be written as

$$\frac{db}{d\hat{z}} = ip - i\kappa(\hat{z})b \quad (1)$$

$$\frac{dp}{d\hat{z}} = -a - i\kappa(\hat{z})p \quad (2)$$

$$\left(\frac{\partial}{\partial \hat{z}} + \frac{1}{2\rho} \frac{\partial}{\partial \theta} \right) a = b \quad (3)$$

In this expression, b is the bunching factor, and p and a are the energy modulation and the radiation field enve-

lope normalized to their saturation values. The normalized longitudinal distance is given by $\hat{z} = 2\rho k_u z$, where z is the distance along the undulator, $k_u = 2\pi/\lambda_u$ is the undulator wavenumber, λ_u is the undulator period, and ρ is the FEL Pierce parameter. Finally, the ponderomotive phase is defined as $\theta = (k_r + k_u)z - \omega_r t$ and can be interpreted as the position along the electron bunch multiplied by the bunching wavenumber $k_r + k_u \simeq k_r$. Furthermore, $\kappa(\hat{z}) = \frac{1}{\rho} \frac{K_0^2}{2 + K_0^2} \Delta(\hat{z})$ is the normalized undulator detuning from the resonance condition, where the peak undulator strength parameter K along the undulator is written as $K(\hat{z}) = K_0(1 + \Delta(\hat{z}))$.

Equations (1)-(3) can be solved analytically for constant and linear tapers $\kappa(\hat{z}) = \kappa_0 + \kappa_1 \hat{z}$ [39]. Here, we consider a general taper $\kappa(\hat{z})$, but suppose that the field interacts weakly with the beam (either due to a significant taper, or a very broad bandwidth seed whose spectral content is mostly non-resonant). In that case, the seed effectively slips over the beam without perturbation from the interaction: $a(\theta, \hat{z}) = a(\theta - \frac{\hat{z}}{2\rho}, 0) \equiv a_0(\theta - \frac{\hat{z}}{2\rho})$ where $a_0(\theta)$ is the initial value of the field at position θ . If we further assume the field to be short so that we can approximately write $a_0(\theta) \simeq A_0 \delta(\theta)$, we find the approximate result for the bunching

$$b(\theta, \hat{z}) = -2\rho i A_0 (\hat{z} - 2\rho\theta) H(\hat{z} - 2\rho\theta) e^{i \int_{\hat{z}}^{2\rho\theta} \kappa(\hat{z}') d\hat{z}'} \quad (4)$$

where $H(x)$ is the Heaviside step function. The θ -dependent phase of the bunching, $\phi = \int_{\hat{z}}^{2\rho\theta} \kappa(x) dx$, encodes the time-frequency chirp induced by the undulator taper. This equation tells us that a given taper profile induces a microbunching spectrotemporal structure of the same qualitative shape, translating the local modulation frequency of the bunching mediated by slippage. For example, a linear taper $\kappa(\hat{z}) = \kappa_1 \hat{z}$ leads to a quadratic phase shift $\phi = \frac{1}{2} \kappa_1 (4\rho^2 \theta^2 - \hat{z}^2) = 2\rho^2 \kappa_1 [(k_r z - \omega_r t)^2 + 2k_u z(k_r z - \omega_r t)]$, which is equivalent to a linear chirp on the bunching.

We will now explore more realistic experimental scenarios using 3D FEL simulations. In the simulations, an electron bunch with constant current is seeded by a 560 eV pulse with 500 attosecond full-width at half-maximum duration (see supplementary information for more simulation details). The undulator lattice geometry is the same as the LCLS-II soft x-ray line, with 87-period segments with a 3.9 cm period. We focus on the seeded physics of the second undulator stage, since the production of isolated attosecond pulses (our seed pulse) has been studied extensively in the past.

The simplest taper profile is a constant undulator strength which may not be resonant with the central frequency of the seed, $K = K_0(1 + \Delta)$. Figure 2 shows (a) the power profile and (b) the output spectrum as a function of the % detuning of the undulators. For each detuning we show the power and spectrum after the undulator length at which the pulse energy has doubled – this choice is made to highlight the characteristics of

experimentally interesting working points. We observe that a second pulse is emitted shortly after the seed with a shifted frequency. This basic process is called “frequency pulling”, which has been studied previously in the asymptotic, long undulator limit [40–42]. Here we are interested in a transient regime where the two pulses coexist [43]. The central frequency of the second pulse is expected to be $\omega_2 = \frac{\sigma_{\omega,s}^2}{\sigma_{\omega,s}^2 + \sigma_{\omega,FEL}^2} (\omega_r - \omega_s)$ [40], where $\sigma_{\omega,s}$ and $\sigma_{\omega,FEL}$ are the bandwidths of the seed and the FEL gain, respectively, and ω_r and ω_s are the resonant frequency in the undulator and the central frequency of the seed, respectively. The FEL bandwidth can be written in terms of the Pierce parameter ρ and the distance into the undulator z as $\sigma_{\omega,FEL} = \omega_r \sqrt{\frac{3\sqrt{3}\rho}{k_u z}}$, where $k_u = 2\pi/\lambda_u$ is the undulator wavenumber (see, for example, [44–46]). The resonant wavelength in the undulator is $\omega_r = \frac{2\gamma^2 k_u c}{1 + K^2}$, where K is the peak undulator strength parameter and γ is the beam Lorentz factor.

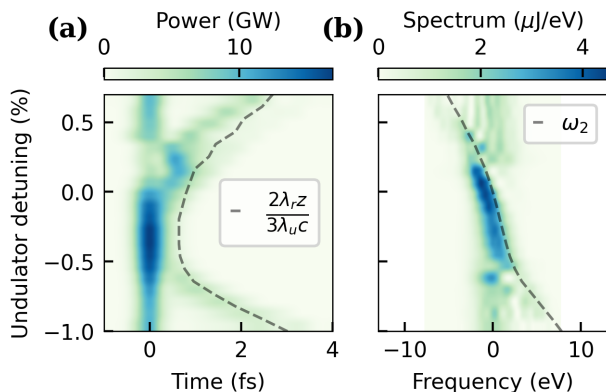


FIG. 2. Simulations of a short seed pulse sliding over a beam in a detuned undulator, with the detuning scanned. (a) The power of the pulse after it has doubled in energy. (b) The spectrum of the pulse after it has doubled in energy. The pulled frequency ω_2 is defined in the text.

The time delay between the two pulses derives from their different group velocities: for large detunings, most of the seed bandwidth falls outside of the FEL gain, so the seed slides over the beam at the speed of light. The secondary pulse, on the other hand, is produced by the usual exponential FEL instability, and moves forward at the FEL group velocity $v_g = c \left(1 - \frac{2\lambda_r}{3\lambda_u}\right)$. In an undulator length z , a temporal delay builds up of value $\Delta t = \frac{2\lambda_r z}{3\lambda_u c}$. This estimate is also shown in panel (a), and we see that it lines up very well with the position of the second pulse for most detunings. For sufficiently small detunings the seed pulse simply gains power from the beam, and can give rise to superradiant behavior [47–50], a case which has been examined in detail in [51].

Delay stages can be used to add more flexible control of the time delay. Such delay stages may be an undulator

detuned far from the resonance, or a dedicated magnetic chicane between undulator segments. Figure 3 shows two applications of delays. In panels (a) and (b), one 87 period section is detuned -0.7% from the K of the first stage, followed by 0, 1, or 2 undulators in a far detuned delay stage mode. The subsequent undulators are set back to the original detuning and allow the pulse energy to double. Panel (b) shows the Wigner distribution of the radiation at the end of this process for the three delay options, and we see from left to right that the primary change is a shifting back of the second pulse by roughly $87 \times \frac{\lambda_r}{c} \simeq 0.64$ fs per additional delay stage with no change to its central frequency. Panels (c) and (d) extend this concept to periodic delays after every undulator section, leading the beam to emit a train of phase-locked attosecond pulses. We scan the delay induced per stage from 0 to 1.5 fs. The power profile is composed of a train of attosecond pulses, and the spectra show fringes with a periodic spacing that decreases as the time spacing increases, as expected for multiple pulses with mutual phase stability.

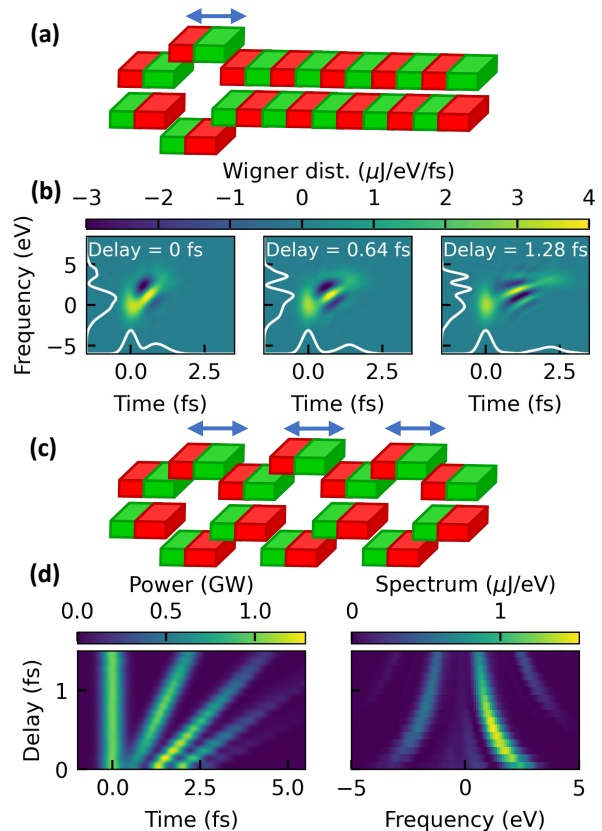


FIG. 3. Simulations of a seed pulse sliding over a detuned undulator section with intermittent delay stages. (a) and (b) are the case of a single delay stage after a short modulating section, with (b) showing the Wigner distributions of the pulse for 0, 1, and 2 undulator sections as delay. (c) and (d) show the case of periodic phase shifters imposing a delay. (d) shows the power and spectrum of the pulse while scanning the delay.

The method described thus far generally yields a sec-

ondary shaped pulse (or train of pulses) while the initial seed pulse is largely unperturbed. To generate isolated shaped pulses, we can leverage harmonic upconversion of the induced microbunching, and radiate at a harmonic of the seed pulse (the seed pulse could be removed by a frequency filter or used in a two-pulse experiment [52]). For the simulations that follow, we now assume a 280 eV seed pulse with 600 attosecond FWHM duration. We note that this pulse duration is representative of the current state of the art, but the coherent bandwidth is not broad enough to directly apply the reasoning used earlier for a δ -function seed. Nevertheless, strategic undulator tapering still yields pulse shaping, as we will now show.

Figure 4 shows three examples. In each case, a linearly tapered undulator imposes roughly linearly chirped microbunching. Following that, a second linearly tapered undulator tuned to the second harmonic of the first prompts lasing at the second harmonic, producing a linearly chirped pulse. Figure 4 panels (c) and (d) show a case leading to a negative linear chirp in the second harmonic pulse, while panels (a)-(b) and (e)-(f) show a case leading to a positive chirp. Beyond simple pulse shaping, this method can produce large spectral bandwidths, as is particularly evident in panels (e) and (f). To place the magnitude of that bandwidth in context, we show the pulse power after it passes through an ideal optical compressor in panel (g), which we simulate by applying a quadratic phase to the field in the frequency domain. We find that the very broad bandwidth linearly chirped pulse could in principle be compressed to 120 as FWHM duration, a factor of four shorter than previously observed with XFELs [30] and five times shorter than the seed.

We conclude by presenting an experimental demonstration of frequency pulling in the pulse pair regime. We performed the experiment at the LCLS using the XLEAP attosecond operating mode [30]. A 4 GeV electron beam was shaped by cathode laser modulation [36]. The undulator is divided in two parts, separated by a magnetic chicane. In the first half of the undulator an isolated attosecond pulse is generated with a 533 eV central photon energy (see supplementary for taper profile). The magnetic chicane imposes a 17 fs delay on the electron beam, overlapping the seed with a fresh electron bunch slice. In the second half of the undulator the seed interacts with the electrons to generate a coherent frequency-pulled pulse. We scan the undulator strength K to change the resonant wavelength in the second section composed of six undulator segments, as in Fig. 2. For each configuration we measured the radiation spectrum using a Variable Line Spacing grating spectrometer [53, 54].

Figure 5(a) shows the average spectrum as a function of undulator strength. There are two notable features: a broad vertical stripe and a narrower stripe which shifts linearly with the undulator detuning. As in our numerical examples (Fig. 2), the broad bandwidth vertical stripe is the spectrum of the seed pulse. The feature which varies with K is the spectrum of the frequency pulled pulse. In panels (b)-(d), we plot five single shot spectra

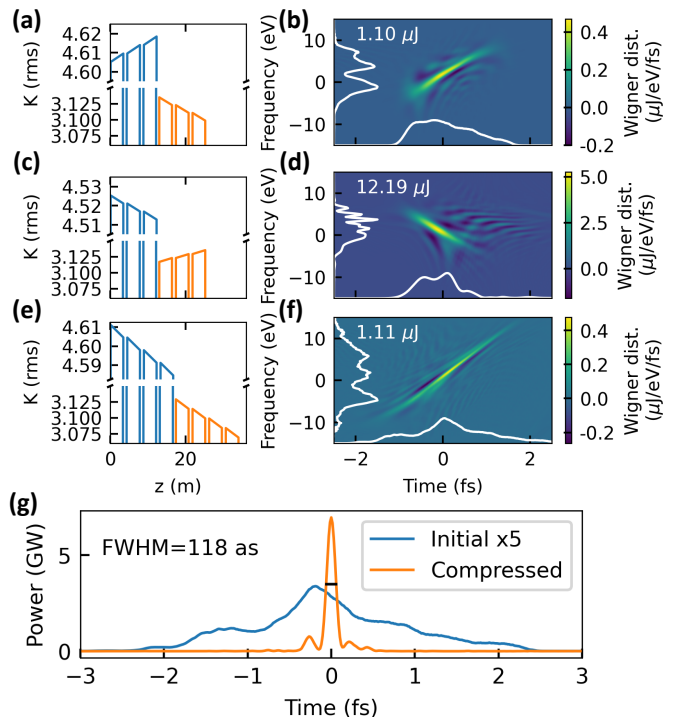


FIG. 4. Simulations of a seed pulse sliding over linear tapered undulators, followed by linearly tapered undulators tuned to the second harmonic of the seed. (b), (d), and (f) show the Wigner distribution of the second harmonic pulse for the undulator tapers shown in (a), (c), and (e), respectively. (g) shows the effect of an ideal pulse compressor on the pulse from (e)-(f).

(in black) as well as the average spectrum (in red) at three different undulator K values (more single shots are shown in the supplementary). The largely single-spike nature of the second lobe confirms that this is due to the emission of a coherent frequency-pulled pulse rather than the presence of a SASE background. We can estimate from our discussion of Fig. 2 that the two pulses are separated by $\frac{2\lambda_r z}{3\lambda_u c} \simeq 2.7$ fs.

In conclusion, we have presented a versatile method for the shaping of attosecond x-ray pulses at free-electron lasers. The method leverages the interplay of slippage and the finite FEL gain bandwidth in order to impose flexible, time-dependent microbunching on the beam that can later lase producing similarly structured attosecond pulses. By combining detuned undulators with delay stages we have shown the possibility to generate phase-locked pulse pairs and pulse trains with controllable temporal spacing and color separation. By leveraging harmonic microbunching, frequency-isolated shaped pulses can be produced and used on their own or combined with the initial attosecond pulse for pump-probe experiments. The exponential seeded FEL gain process allows us to generate very large coherent bandwidths in this way, paving a path towards 100 as soft x-ray pulse durations for the first time. Finally, we have demon-

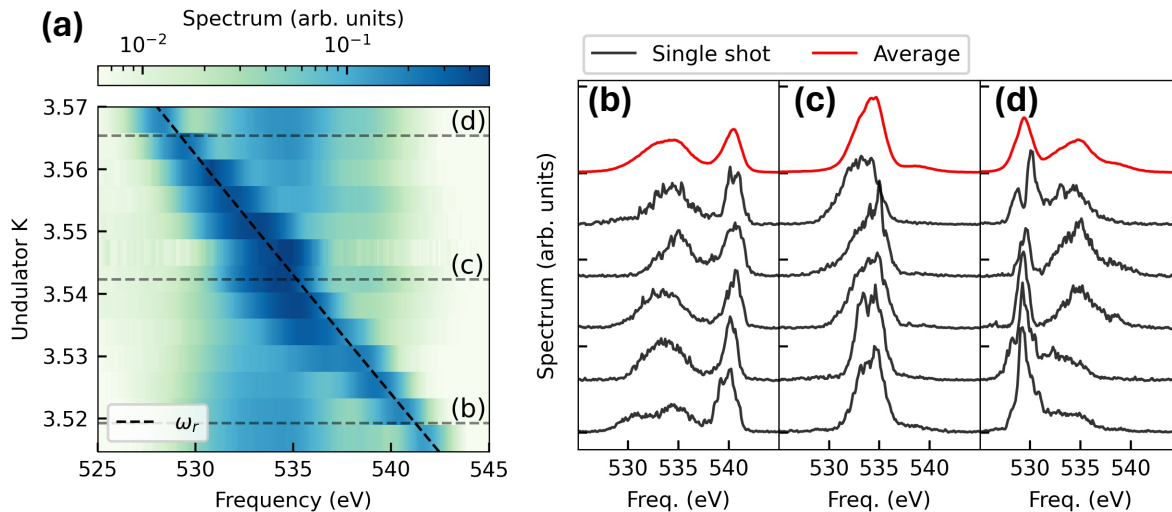


FIG. 5. Spectra from experimental demonstration of frequency pulling. (a) The average spectrum versus undulator K , plotted alongside the resonant frequency. (b)-(d) show single shot spectra in black at three K values indicated in panel (a), and the average spectrum in red.

strated the simplest of the shaping methods, pulse pairs by frequency pulling, at the LCLS. The experiment was conducted using an enhanced SASE method driven by photo-cathode laser modulation. The experiment reproduces the spectral features observed in our simulations of frequency pulling and showcases the ability to reshape attosecond x-ray pulses from XFELs.

This work was supported by the U.S. Department of

Energy, Office of Science, Office of Basic Energy Sciences under Contract No. DE-AC02-76SF00515, and by the U.S. Department of Energy, Office of Science, Office of Basic Energy Sciences Accelerator and Detector Research Program. R. R. R. acknowledges the support of the Stanford Graduate Fellowship and the Robert H. Siemann Fellowship. The authors thank Zhirong Huang for helpful discussions.

-
- [1] A. M. Weiner, J. P. Heritage, and E. Kirschner, High-resolution femtosecond pulse shaping, *JOSA B* **5**, 1563 (1988).
- [2] C. W. Hillegas, J. X. Tull, D. Goswami, D. Strickland, and W. S. Warren, Femtosecond laser pulse shaping by use of microsecond radio-frequency pulses, *Optics Letters* **19**, 737 (1994).
- [3] A. M. Weiner, Femtosecond pulse shaping using spatial light modulators, *Review of scientific instruments* **71**, 1929 (2000).
- [4] S.-H. Shim, D. B. Strasfeld, E. C. Fulmer, and M. T. Zanni, Femtosecond pulse shaping directly in the mid-ir using acousto-optic modulation, *Optics letters* **31**, 838 (2006).
- [5] A. M. Weiner, Ultrafast optical pulse shaping: A tutorial review, *Optics Communications* **284**, 3669 (2011).
- [6] P. Maine, D. Strickland, P. Bado, M. Pessot, and G. Mourou, Generation of ultrahigh peak power pulses by chirped pulse amplification, *IEEE Journal of Quantum electronics* **24**, 398 (1988).
- [7] P. Brumer and M. Shapiro, Control of unimolecular reactions using coherent light, *Chemical physics letters* **126**, 541 (1986).
- [8] S. Shi, A. Woody, and H. Rabitz, Optimal control of selective vibrational excitation in harmonic linear chain molecules, *The Journal of chemical physics* **88**, 6870 (1988).
- [9] R. Kosloff, S. A. Rice, P. Gaspard, S. Tersigni, and D. Tannor, Wavepacket dancing: Achieving chemical selectivity by shaping light pulses, *Chemical Physics* **139**, 201 (1989).
- [10] D. Goswami, Optical pulse shaping approaches to coherent control, *Physics Reports* **374**, 385 (2003).
- [11] K. Ohmori, Wave-packet and coherent control dynamics, *Annual review of physical chemistry* **60**, 487 (2009).
- [12] R. Bonifacio, C. Pellegrini, and L. Narducci, Collective instabilities and high-gain regime in a free electron laser, *Optics Communications* **50**, 373 (1984).
- [13] P. Emma, R. Akre, J. Arthur, R. Bionta, C. Bostedt, J. Bozek, A. Brachmann, P. Bucksbaum, R. Coffee, F.-J. Decker, *et al.*, First lasing and operation of an ångstrom-wavelength free-electron laser, *nature photonics* **4**, 641 (2010).
- [14] E. Allaria, R. Appio, L. Badano, W. Barletta, S. Bassanese, S. Biedron, A. Borga, E. Busetto, D. Castronovo, P. Cinquegrana, *et al.*, Highly coherent and stable pulses from the fermi seeded free-electron laser in the extreme ultraviolet, *Nature Photonics* **6**, 699 (2012).
- [15] L.-H. Yu, M. Babzien, I. Ben-Zvi, L. DiMauro, A. Doyuran, W. Graves, E. Johnson, S. Krinsky, R. Malone,

- I. Pogorelsky, *et al.*, High-gain harmonic-generation free-electron laser, *Science* **289**, 932 (2000).
- [16] L. H. Yu, L. DiMauro, A. Doyuran, W. Graves, E. Johnson, R. Heese, S. Krinsky, H. Loos, J. Murphy, G. Rakowsky, *et al.*, First ultraviolet high-gain harmonic-generation free-electron laser, *Physical review letters* **91**, 074801 (2003).
- [17] D. Xiang and G. Stupakov, Echo-enabled harmonic generation free electron laser, *Physical Review Special Topics-Accelerators and Beams* **12**, 030702 (2009).
- [18] D. Xiang, E. Colby, M. Dunning, S. Gilevich, C. Hast, K. Jobe, D. McCormick, J. Nelson, T. Raubenheimer, K. Soong, *et al.*, Demonstration of the echo-enabled harmonic generation technique for short-wavelength seeded free electron lasers, *Physical review letters* **105**, 114801 (2010).
- [19] Z. Zhao, D. Wang, J. Chen, Z. Chen, H. Deng, J. Ding, C. Feng, Q. Gu, M. Huang, T. Lan, *et al.*, First lasing of an echo-enabled harmonic generation free-electron laser, *Nature Photonics* **6**, 360 (2012).
- [20] D. Gauthier, P. R. Ribič, G. De Ninno, E. Allaria, P. Cinquegrana, M. B. Danailov, A. Demidovich, E. Ferrari, L. Giannessi, B. Mahieu, *et al.*, Spectrotemporal shaping of seeded free-electron laser pulses, *Physical review letters* **115**, 114801 (2015).
- [21] P. K. Maroju, C. Grazioli, M. Di Fraia, M. Moioli, D. Ertel, H. Ahmadi, O. Plekan, P. Finetti, E. Allaria, L. Giannessi, *et al.*, Attosecond pulse shaping using a seeded free-electron laser, *Nature* **578**, 386 (2020).
- [22] K. Prince, E. Allaria, C. Callegari, R. Cucini, G. De Ninno, S. Di Mitri, B. Diviacco, E. Ferrari, P. Finetti, D. Gauthier, *et al.*, Coherent control with a short-wavelength free-electron laser, *Nature Photonics* **10**, 176 (2016).
- [23] P. K. Maroju, M. Di Fraia, O. Plekan, M. Bonanomi, B. Merzuk, D. Busto, I. Makos, M. Schmoll, R. Shah, P. R. Ribič, *et al.*, Attosecond coherent control of electronic wave packets in two-colour photoionization using a novel timing tool for seeded free-electron laser, *Nature Photonics* **17**, 200 (2023).
- [24] D. Gauthier, E. Allaria, M. Coreno, I. Cudin, H. Dacasa, M. B. Danailov, A. Demidovich, S. Di Mitri, B. Diviacco, E. Ferrari, *et al.*, Chirped pulse amplification in an extreme-ultraviolet free-electron laser, *Nature communications* **7**, 13688 (2016).
- [25] A. Marinelli, D. Ratner, A. Lutman, J. Turner, J. Welch, F.-J. Decker, H. Loos, C. Behrens, S. Gilevich, A. Miahnahri, *et al.*, High-intensity double-pulse x-ray free-electron laser, *Nature communications* **6**, 6369 (2015).
- [26] A. A. Lutman, T. J. Maxwell, J. P. MacArthur, M. W. Guetg, N. Berrah, R. N. Coffee, Y. Ding, Z. Huang, A. Marinelli, S. Moeller, *et al.*, Fresh-slice multicolour x-ray free-electron lasers, *Nature Photonics* **10**, 745 (2016).
- [27] Y. Ding, R. Coffee, F.-J. Decker, P. Emma, C. Field, W. Helml, Z. Huang, P. Krejčík, J. Krzywinski, *et al.*, Generating femtosecond x-ray pulses using an emittance-spoiling foil in free-electron lasers, *Applied Physics Letters* **107** (2015).
- [28] A. Marinelli, R. Coffee, S. Vetter, P. Hering, G. West, S. Gilevich, A. Lutman, S. Li, T. Maxwell, J. Galayda, *et al.*, Optical shaping of x-ray free-electron lasers, *Physical review letters* **116**, 254801 (2016).
- [29] J. P. Duris, J. P. MacArthur, J. M. Glowonia, S. Li, S. Vetter, A. Miahnahri, R. Coffee, P. Hering, A. Fry, M. E. Welch, *et al.*, Controllable x-ray pulse trains from enhanced self-amplified spontaneous emission, *Physical Review Letters* **126**, 104802 (2021).
- [30] J. Duris, S. Li, T. Driver, E. G. Champenois, J. P. MacArthur, A. A. Lutman, Z. Zhang, P. Rosenberger, J. W. Aldrich, R. Coffee, *et al.*, Tunable isolated attosecond x-ray pulses with gigawatt peak power from a free-electron laser, *Nature Photonics* **14**, 30 (2020).
- [31] E. Prat, A. Al Haddad, C. Arrell, S. Augustin, M. Boll, C. Bostedt, M. Calvi, A. L. Cavalieri, P. Craievich, A. Dax, *et al.*, An x-ray free-electron laser with a highly configurable undulator and integrated chicanes for tailored pulse properties, *Nature communications* **14**, 5069 (2023).
- [32] S. Huang, Y. Ding, Y. Feng, E. Hemsing, Z. Huang, J. Krzywinski, A. Lutman, A. Marinelli, T. Maxwell, and D. Zhu, Generating single-spike hard x-ray pulses with nonlinear bunch compression in free-electron lasers, *Physical review letters* **119**, 154801 (2017).
- [33] J. T. O'Neal, E. G. Champenois, S. Oberli, R. Obaid, A. Al-Haddad, J. Barnard, N. Berrah, R. Coffee, J. Duris, G. Galinis, *et al.*, Electronic population transfer via impulsive stimulated x-ray raman scattering with attosecond soft-x-ray pulses, *Physical review letters* **125**, 073203 (2020).
- [34] T. Tanaka, Proposal to generate an isolated monochromatic x-ray pulse by counteracting the slippage effect in free-electron lasers, *Physical Review Letters* **114**, 044801 (2015).
- [35] S. Li, T. Driver, P. Rosenberger, E. G. Champenois, J. Duris, A. Al-Haddad, V. Averbukh, J. C. Barnard, N. Berrah, C. Bostedt, *et al.*, Attosecond coherent electron motion in auger-meitner decay, *Science* **375**, 285 (2022).
- [36] Z. Zhang, J. Duris, J. P. MacArthur, A. Zholtens, Z. Huang, and A. Marinelli, Experimental demonstration of enhanced self-amplified spontaneous emission by photocathode temporal shaping and self-compression in a magnetic wiggler, *New Journal of Physics* **22**, 083030 (2020).
- [37] D. Cesar, A. Anakru, S. Carbajo, J. Duris, P. Franz, S. Li, N. Sudar, Z. Zhang, and A. Marinelli, Electron beam shaping via laser heater temporal shaping, *Physical Review Accelerators and Beams* **24**, 110703 (2021).
- [38] J. P. MacArthur, J. Duris, Z. Zhang, A. Lutman, A. Zholtens, X. Xu, Z. Huang, and A. Marinelli, Phase-stable self-modulation of an electron beam in a magnetic wiggler, *Physical Review Letters* **123**, 214801 (2019).
- [39] P. Baxevanis, J. Duris, Z. Huang, and A. Marinelli, Time-domain analysis of attosecond pulse generation in an x-ray free-electron laser, *Physical Review Accelerators and Beams* **21**, 110702 (2018).
- [40] E. Allaria, M. Danailov, and G. De Ninno, Tunability of a seeded free-electron laser through frequency pulling, *Europhysics Letters* **89**, 64005 (2010).
- [41] E. Allaria, G. De Ninno, and C. Spezzani, Experimental demonstration of frequency pulling in single-pass free-electron lasers, *Optics Express* **19**, 10619 (2011).
- [42] N. S. Mirian, M. Di Fraia, S. Spampinati, F. Sottocorona, E. Allaria, L. Badano, M. B. Danailov, A. Demidovich, G. De Ninno, S. Di Mitri, *et al.*, Generation and measurement of intense few-femtosecond superradiant extreme-ultraviolet free-electron laser pulses, *Nature Photonics* **15**, 523 (2021).

- [43] R. Robles *et al.*, Attosecond pulse shaping of X-ray free-electron lasers and applications to coherent control in quantum systems (JACoW Publishing, Geneva, Switzerland) presented at IPAC'23, Venice, Italy, May 2023, paper TUPL094.
- [44] Z. Huang and K.-J. Kim, Review of x-ray free-electron laser theory, *Physical Review Special Topics-Accelerators and Beams* **10**, 034801 (2007).
- [45] C. Pellegrini, A. Marinelli, and S. Reiche, The physics of x-ray free-electron lasers, *Reviews of Modern Physics* **88**, 015006 (2016).
- [46] K.-J. Kim, Z. Huang, and R. Lindberg, *Synchrotron radiation and free-electron lasers* (Cambridge university press, 2017).
- [47] R. Bonifacio and F. Casagrande, The superradiant regime of a free electron laser, *Nuclear Instruments and Methods in Physics Research Section A: Accelerators, Spectrometers, Detectors and Associated Equipment* **239**, 36 (1985).
- [48] R. Bonifacio, B. McNeil, and P. Pierini, Superradiance in the high-gain free-electron laser, *Physical Review A* **40**, 4467 (1989).
- [49] R. Bonifacio, N. Piovella, and B. McNeil, Superradiant evolution of radiation pulses in a free-electron laser, *Physical Review A* **44**, R3441 (1991).
- [50] L. Giannessi, P. Musumeci, and S. Spampinati, Nonlinear pulse evolution in seeded free-electron laser amplifiers and in free-electron laser cascades, *Journal of Applied Physics* **98** (2005).
- [51] P. Franz *et al.*, Terawatt-scale attosecond x-ray pulses from a cascaded superradiant free-electron laser, *Accepted by Nature Photonics* (2024).
- [52] Z. Guo *et al.*, Experimental demonstration of attosecond pump-probe spectroscopy with an x-ray free-electron laser, *Accepted by Nature Photonics* (2024).
- [53] M. C. Hettrick, J. H. Underwood, P. J. Batson, and M. J. Eckart, Resolving power of 35,000 (5 ma) in the extreme ultraviolet employing a grazing incidence spectrometer, *Applied optics* **27**, 200 (1988).
- [54] Y.-D. Chuang, Y.-C. Shao, A. Cruz, K. Hanzel, A. Brown, A. Frano, R. Qiao, B. Smith, E. Domning, S.-W. Huang, *et al.*, Modular soft x-ray spectrometer for applications in energy sciences and quantum materials, *Review of Scientific Instruments* **88** (2017).

Supplementary Information: Spectrotemporal shaping of attosecond x-ray pulses with a fresh-slice free-electron laser

River R. Robles,^{1,2,3,*} Kirk A. Larsen,^{1,3,†} David Cesar,¹ Taran Driver,^{1,3} Joseph Duris,¹ Paris Franz,^{1,2,3} Douglas Garratt,^{1,3} Nicholas Sudar,¹ Jun Wang,^{1,2,3} Zhen Zhang,¹ James Cryan,^{1,3,‡} and Agostino Marinelli^{1,3,§}

¹*SLAC National Accelerator Laboratory, Menlo Park, CA 94025*

²*Stanford University, Department of Applied Physics, Stanford, CA 94305*

³*Stanford PULSE Institute, SLAC National Accelerator Laboratory, Menlo Park, CA 94025, USA*

(Dated: March 5, 2024)

arXiv:2403.02189v1 [physics.acc-ph] 4 Mar 2024

* riverr@stanford.edu

† larsenk@stanford.edu

‡ jcryan@slac.stanford.edu

§ marinelli@slac.stanford.edu

I. SIMULATION DETAILS

The relevant parameters for all simulations are shown in Table I. The values without parentheses are relevant for the multi-pulse simulations (Figures 2 and 3 in the main text) except for the peak power for the pulse trains portion of Figure 3, for which the power is given in brackets in the table. The values in parentheses are relevant for Figure 4.

| Beam parameter | Value |
|----------------------|--------------------------|
| Current | 2 kA |
| Average beam size | 20 μm |
| Normalized emittance | 0.4 μm |
| Energy | 5 GeV |
| Energy spread | 2 MeV |
| Undulator parameter | Value |
| Period | 3.9 cm |
| Periods per segment | 87 |
| Seed field parameter | Value |
| Central frequency | 560 (280) eV |
| FWHM power duration | 0.5 (0.6) fs |
| Peak power | 10 [1] GW |
| Spot size w_0 [?] | 70.7 (100) μm |

TABLE I: Parameters for simulations. Meanings of parentheses and brackets are explained in the text.

In the pulse pair simulations with delays (Figure 3), the delay stages are undulator segments detuned 4% in K . In the pulse train simulations, the delay stages are represented by phase shifters between segments. To clean up the temporal profile of the train we applied, in addition to the macroscopic delay, a π phase shift at each phase shifter. Furthermore, we found that the undulator segments in the LCLS-II lattice were long enough that sufficient gain occurred to distort the temporal profile. To clean up these effects, we linearly tapered each individual segment so as to reduce the coupling between the beam and the radiation, effectively shortening the segment.

II. EXPERIMENT DETAILS

The experiment was performed at the LCLS soft x-ray undulator line. Seven undulator segments, each 87 periods long, were set to a linear taper to match a large linear chirp in a current spike in the driving electron beam. Subsequently, a chicane delayed the electron beam by 17 femtoseconds. This both washed out any residual microbunching in the current spike and overlapped the x-ray pulse produced in the first stage with fresh electrons. The beam lased, seeded by the seed from the first stage, in six subsequent undulator segments. Typical taper profiles are shown in Figure S1. The first stage was not changed while the second stage was scanned.

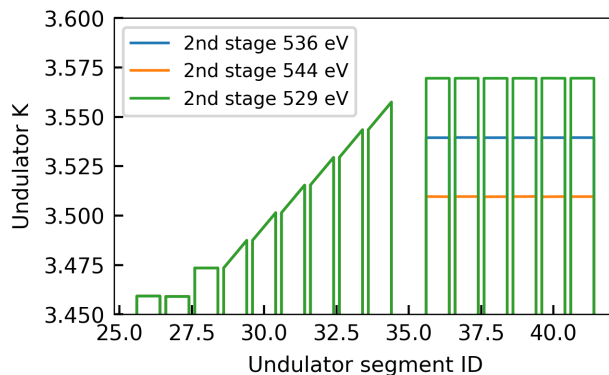


FIG. S1: Experimental undulator K values for three different central photon energies in the second stage.

The spectrum at the output of the second stage was measured using a Variable Line Spacing (VLS) grating spectrometer [? ?] in the chemRIXS/qRIXS experimental end station. In addition to the single shot spectra shown in the main paper, we show additional single shot spectra in Figure S2 for three different K values in the second stage. We note that the higher photon energy working point shown in panel (a) exhibits a consistent single spike secondary

pulse at 543 eV photon energy. More spectral splitting is observed at the lower photon energy around 530 eV in panel (c), which is not unexpected when two phase-stable fields with spectral and temporal delays are added coherently.

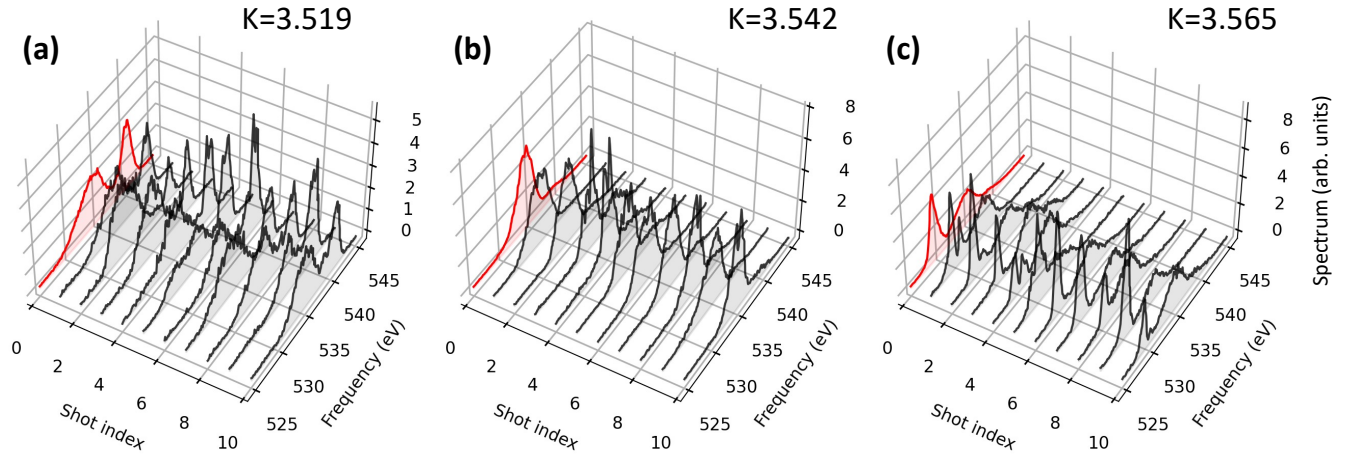


FIG. S2: Ten single shots are plotted for each of three different second stage K values as well as their average.

Figure S3 shows the measured pulse energy as a function of the K of the second stage, with blue dots representing single shots and a black line indicating the average at each bin in K . Most of the pulse energy is generated in the first stage which is independent of the K in the second stage. The dependence of the measured pulse energy on K is indicative of the seeded nature of the second stage.

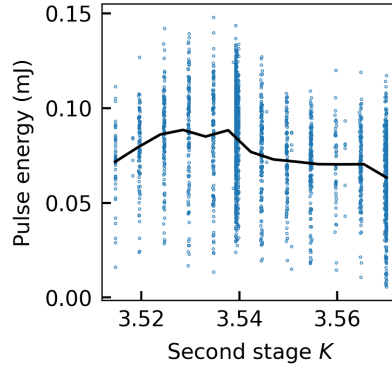


FIG. S3: Pulse energies measured in the experiment versus undulator strength K in the second stage.